THE JOURNAL OF BIOLOGICAL CHEMISTRY
Vol. 279, No. 28, Issue of July 9, pp. 28945–28953, 2004
Printed in U.S.A.

Operator Design and Mechanism for CarA Repressor-mediated Down-regulation of the Photoinducible *carB* Operon in *Myxococcus xanthus**

Received for publication, March 29, 2004
Published, JBC Papers in Press, April 28, 2004, DOI 10.1074/jbc.M403459200

José Juan López-Rubio‡§, S. Padmanabhan‡, Jose María Lázaro¶, Margarita Salas¶, Francisco José Murillo‡‖, and Montserrat Elías-Arnanz‡**

From the ‡Departamento de Genética y Microbiología, Facultad de Biología, Universidad de Murcia, Murcia 30071, and the ¶Centro de Biología Molecular-Severo Ochoa, Universidad Autónoma, Cantoblanco, Madrid 28049, Spain

The *carB* operon encodes all except one of the enzymes involved in light-induced carotenogenesis in *Myxococcus xanthus*. Expression of its promoter (P_B) is repressed in the dark by sequence-specific DNA binding of CarA to a palindrome (pI) located between positions −47 and −64 relative to the transcription start site. This promotes subsequent binding of CarA to additional sites that remain to be defined. CarS, produced in the light, interacts physically with CarA, abrogates CarA-DNA binding, and thereby derepresses P_B. In this study, we delineate the operator design that exists for CarA by precisely mapping out the second operator element. For this, we examined how stepwise deletions and site-directed mutagenesis in the region between the palindrome and the transcription start site affect CarA binding around P_B *in vitro* and expression of P_B *in vivo*. These revealed the second operator element to be an imperfect interrupted palindrome (pII) spanning positions −26 to −40. *In vitro* assays using purified *M. xanthus* RNA polymerase showed that CarA abolishes P_B-RNA polymerase binding and runoff transcription and that both were restored by CarS, thus rationalizing the observations *in vivo*. CarA binding to pII (after association with pI) effectively occludes RNA polymerase from P_B and so provides the operative mechanism for the repression of the *carB* operon by CarA. The bipartite operator design, whereby transcription is blocked by the low affinity CarA-pII binding and is readily restored by CarS, may have evolved to match the needs for a rapid and an effective response to light.

Bacteria typically adapt to changing environmental conditions by switching on or off the expression of specific subsets of genes. Transcription initiation is the principal stage at which bacterial gene expression is regulated (for review, see Refs. 1 and 2). Initiation of transcription at a given promoter is a multistep process that begins with the recognition of the promoter by RNA polymerase (RNAP)[1] holoenzyme guided at this step by specific σ factors. The "closed" binary complex formed by the initial binding of RNAP to the promoter is then stabilized by local DNA melting to form an "open" complex. In the presence of the four ribonucleotides, an initial transcribing complex is formed that eventually leaves the promoter as a productive elongation complex. Any of these steps in transcription initiation can be targeted for negative regulation by specific transcription factors. In the classical sense, phage repressors such as those of λ and 434 (3), or the *Escherichia coli lac* repressor (see Ref. 4), bind to operator sites that overlap the RNAP recognition elements. Repressor-operator binding can therefore serve as a physical block to RNAP-promoter binding as long as the operator binding affinity of the repressor exceeds that of RNAP for its promoter. Variations on this theme include binding to a site outside the promoter region, which then favors the propagation of multiply bound repressor complexes that come to occupy regions within the promoter and thereby occlude RNAP (5). Alternatively, the repressor may alter the DNA structure in a manner that makes the promoter refractory to RNAP binding (6, 7). Transcription initiation can nevertheless be impaired at a step after closed complex formation. This is usually achieved by repressors that coexist with RNAP on DNA and whose binding sites may or may not overlap. Examples include repressors that interfere with the isomerization to the open complex (8–10), the formation of the initial transcribing complex (11), or promoter clearance (12).

Transcriptional regulation of light-induced carotenogenesis in the bacterium *Myxococcus xanthus* is the focus of our work. Blue light switches on a regulatory cascade in *M. xanthus* that culminates in the synthesis of carotenoids, a major class of pigments that protect cells against photo-oxidative damage (13). The known circuits in the light-induced carotenogenesis in *M. xanthus* are schematically shown in Fig. 1. The *carB* operon constitutes one of two distinct genetic loci (the other being the unlinked *crtI*) involved in expressing the enzymes required for carotenoid synthesis. Six of these enzymes are encoded by this operon and only one by *crtI* (14–16). *carF* is a recently identified gene whose product has been proposed to function as an anti-anti-σ factor at the earliest step in the regulatory cascade (17). The *carQRS* locus is a key regulatory operon that encodes three proteins with low, basal levels of expression in the dark: the extracytoplasmic function σ-factor CarQ (18–20), its anti-σ factor CarR (18, 20), and the antirepressor protein CarS (21, 22). Central to the induction of carotenogenesis on exposure to

* This work was supported in part by Grants BMC2000-1006 (to F. J. M.), BMC2002-03818 (to M. S.), and BMC2002-00539 and Programa Ramón y Cajal (to S. P.) from the Ministerio de Ciencia y Tecnología, Spain. The costs of publication of this article were defrayed in part by the payment of page charges. This article must therefore be hereby marked "*advertisement*" in accordance with 18 U.S.C. Section 1734 solely to indicate this fact.

§ Supported by a fellowship from Fundación Séneca (Murcia-Spain).

‖ To whom correspondence may be addresssed. Tel.: 34-968-364-951; Fax: 34-968-363-963; E-mail: araujo@um.es.

** To whom correspondence may be addressed. Tel.: 34-968-367-134; Fax: 34-968-363-963; E-mail: melias@um.es.

[1] The abbreviations used are: RNAP, RNA polymerase; EMSA, electrophoretic mobility shift assay; MxRNAP, *M. xanthus* RNAP; P_B, *carB* promoter.

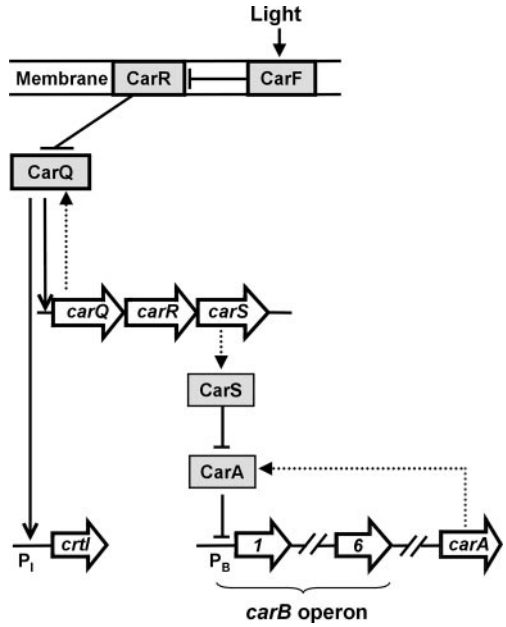

FIG. 1. **Light-induced carotenogenesis in *M. xanthus*.** The cast of factors identified thus far is shown. Genes/open reading frames (*orf′s*) are indicated by the *squat arrows*, proteins as *rectangles shaded gray*, positive regulation by *continuous arrows*, and negative regulation by *blunt ended lines*. Enzymes involved in carotenoid biosynthesis are encoded by the gene *crtI* and the six genes of the *carB* operon, whose respective promoters P_I and P_B are light-inducible. *orf10* in the *carA* operon codes for the constitutively expressed CarA, and the photoinducible *carQRS* operon codes for CarQ (an ECF σ factor), CarR (a membrane protein), and CarS (the antirepressor of CarA). CarF (likely a membrane protein) is involved in the light-driven inactivation of CarR. Other essential protein factors that are implicated in the process, and not shown in the figure, are the constitutively expressed CarD (a high mobility group A-like protein) and IhfA (integration host factor α subunit).

light is the CarF-mediated inactivation of CarR to release CarQ (17, 18). Once liberated, CarQ up-regulates expression of *carQRS* and *crtI* (18). In this, CarQ is aided by the high mobility group A-type protein CarD (23–26) and the histone-like protein IhfA (integration host factor α subunit) (27). The photo-induced expression of the *carB* operon is regulated by CarA, which is produced independently of light from an adjacent operon, and by CarS (28, 29). In the dark, *carB* is repressed by the sequence-specific binding of CarA to a DNA stretch that includes an interrupted palindrome located upstream of the *carB* promoter (P_B) (22). Illumination leads to an increase in the levels of CarS, which physically interacts with CarA, and thereby dismantles the CarA·DNA complex to cause derepression of *carB* (21, 22). Our previous study identified the palindrome that is present upstream of P_B (between positions −47 and −64 relative to the transcription start point) as an essential element of the CarA operator. We had also presented evidence that binding to this palindrome somehow aided CarA in reaching out to additional sites that lie within P_B, but the details of this remained to be elucidated. In this study we delineate the operator design employed by the *M. xanthus* CarA repressor and examine how the repression of the *carB* operon is brought about. The additional elements that constitute the CarA operator were sought by systematic truncations and site-directed mutagenesis of the DNA probe used in CarA·DNA binding assays *in vitro*. The consequences of the specific mutations in the operator region on *carB* expression *in vivo* were also investigated. Furthermore, we studied the molecular basis for the CarA-mediated down-regulation of P_B using purified *M. xanthus* RNAP (MxRNAP) in DNA binding and runoff transcription assays *in vitro* and how this was affected by CarS. Based on these we define all of the CarA operator elements and provide a mechanistic model for how CarA may repress *carB* expression.

EXPERIMENTAL PROCEDURES

Bacterial Strains and Growth Conditions—The wild-type *M. xanthus* strain used in this study was DK1050 (30). *M. xanthus* cells were grown in the rich medium casitone-Tris (31). *E. coli* strain DH5α was used for plasmid constructions, BL21(DE3) (pLysS) for protein overexpression, and Luria broth as the growth medium (32).

Overexpression and Purification of His-tagged CarA and CarS—Plasmid constructs for overexpressing His_6-tagged CarA and CarS, their overexpression, purification, and concentration determination have been described previously (22). His_6-CarS was expressed as a soluble protein and purified under native conditions. A small amount of the partially soluble His_6-CarA was purified under native conditions, but most was purified under denaturing solution conditions followed by renaturation. Both His_6-CarA preparations gave identical results when examined separately; the fraction used in the *in vitro* assays described here was the one purified under native conditions.

Purification of M. xanthus RNA Polymerase—*M. xanthus* strain DK1050 was grown to mid-log phase in casitone-Tris medium, and the cells (~5 g wet weight/liter of culture) were collected by centrifugation. Pelleted cells were frozen at −70 °C before being used. The MxRNAP holoenzyme was purified under ice-cold conditions using a modification of the protocol described by Rudd and Zusman (33). Frozen cells (~29 g wet weight) were broken with alumina (~2 g/g cell pellet) in a minimal amount of grinding buffer (buffer A (50 mM Tris, pH 7.5, 1 mM EDTA, 7 mM β-mercaptoethanol, 5% glycerol) plus 0.35 M NaCl) and 0.1 ml each of 100 mM phenylmethylsulfonyl fluoride, 100 mM benzamidine, and protease inhibitor mixture (Sigma). Lysed cells were suspended in 180 ml of grinding buffer and centrifuged at 500 × *g* for 10 min to remove alumina. The resulting supernatant was centrifuged at 17,500 × *g* for 15 min, and the process was repeated to obtain the final debris-free supernatant. The latter was mixed with polyethyleneimine to a final concentration of 0.3%, incubated on ice for 20 min, and centrifuged (17,500 × *g*, 15 min). The polyethyleneimine pellet was washed with 56 ml of buffer A containing 1 M NaCl, 0.04% polyethyleneimine, and the above protease inhibitor mix, incubated, and centrifuged as before, and the pellet was subjected to a second 28-ml wash with the same solution. The washes were pooled and processed by stepwise ammonium sulfate precipitation at 58%, 47.5%, and finally 35%. Proteins were recovered from the 35% ammonium sulfate supernatant by raising it to 60% ammonium sulfate. This last pellet was resuspended in buffer A to a final salt concentration of 0.25 M (estimated by conductivity measurements) and loaded onto a 17-ml heparin column preequilibrated with buffer A plus 0.25 M NaCl. To the column was then applied ~5–7 times its volume of buffer A containing 0.25, 0.3, 0.4, and 0.5 M NaCl. Fractions containing MxRNAP (as determined by SDS-PAGE) were pooled, diluted with an equal volume of buffer A, and applied to a 12-ml double-stranded DNA-cellulose column preequilibrated with buffer A containing 0.25 M NaCl and eluted with 0.6 M NaCl. Fractions containing MxRNAP were pooled, precipitated with ammonium sulfate, resuspended in buffer A containing 50% glycerol, and stored at −70 °C. Western blots employing polyclonal antibodies raised against the *Bacillus subtilis* RNAP holoenzyme were used to verify that the purified MxRNAP holoenzyme contained the major *M. xanthus* vegetative σ^A (80 kDa; apparent size of 105 kDa), α (43 kDa) and β/β' subunits (at ~150 kDa). The presence of σ^A was further confirmed using *B. subtilis* polyclonal anti-σ-43 antibodies (34, 35). The final MxRNAP concentration estimated using the Bio-Rad protein assay was 3.5 μg/μl.

Gel Mobility Shift and DNase I Footprinting Assays—PCRs with one of the two primers radiolabeled at the 5′-end were carried out to generate the DNA probes (22). Probes with specific mutations were obtained by the PCR overlap extension method (36). Binding was performed at 37 °C for 30 min in a 20-μl reaction volume containing 100 mM KCl, 25 mM Tris, pH 8, 5 mM $MgCl_2$, 1 mM dithiothreitol, 10% glycerol, 200 ng/μl bovine serum albumin, 1 μg of poly(dI-dC) as nonspecific competitor, ~1 nM end-labeled double-stranded probe (~13,000 cpm), and the indicated amounts of proteins. In reactions containing both CarA and MxRNAP, the DNA probe was preincubated with CarA at 37 °C for 30 min, then MxRNAP was added and incubation continued for an additional 30 min, unless otherwise stated. When CarS was also present, it was added simultaneously with CarA. Reactions were loaded onto 4% nondenaturing polyacrylamide gels (acrylamide:bisacrylamide 37.5:1) pre-run at 200 V/10 °C for 30 min in 0.5 × TBE buffer (45 mM

TABLE I
DNA probes used in this study

Name	Sequence[a]
	D1 ←---------- D2 ←----------
	−70 ——→ pI ←—— −40 ——→pII ←—— −10
CCR209	5′-..GTACAAGGTTAT*CGCAAACCTTA*GACATACCC**TTGACA**AGCTCTGGA*CGCAAACGC**TACCTC**TAGG..(+107)-3′
CCR130	5′-..GTACAAGGTTAT*CGCAAACCTTA*GACATACCC**TTGACA**AGCTCTGGA*CGCAAACGC**TACCTC**TAGG..(+28)-3′
CCR98	5′-..GTACAAGGTTAT*CGCAAACCTTA*GACATACCC**TTGACA**AGCTCTGGA*CGCAAACGC**TACCTC**TA-3′
CCR87	5′-..GTACAAGGTTAT*CGCAAACCTTA*GACATACCC**TTGACA**AGCTCTGGA*CGCAAA*-3′
CCR81	5′-..GTACAAGGTTAT*CGCAAACCTTA*GACATACCC**TTGACA**AGCTCTGGA-3′
CCR64	5′-..GTACAAGGTTAT*CGCAAACCTTA*GACATACCC-3′
CCR76	5′-*TT*AGACATACCC**TTGACA**AGCTCTGGA*CGCAAACGC**TACCTC**TAGG...3′
CCR130-DMUT2	5′-..GTACAAGGTTAT*CGCAAACCTTA*GACATACCC**TTGACA**AGCTCTGGA*tcagAACGC**TACCTC**TAGG...3′
CCR130-DMUT3	5′-..GTACAAGGTTAT*CGCAAACCTTA*GACATACCC**TTGACA**AGCTCTGGA*CGCAccaGC**TACCTC**TAGG...3′
CCR130-pIImut1	5′-..GTACAAGGTTAT*CGCAAACCTTA*GACATcCqC**TTGACA**AtCcCTGGA*CGCAAACGC**TACCTC**TAGG...3′
CCR76-pIImut1	5′-*TT*AGACATcCqC**TTGACA**AtCcCTGGA*CGCAAACGC**TACCTC**TAGG...3′

[a] The sequence of only one strand is shown. The −10 and −35 promoter elements are in boldface. The CarA operator elements pI (−64 to −47) and pII (−40 to −26) are underlined and marked with solid arrows. The two direct repeats D1 (−56 to −46) and D2 (−21 to −11) are in italics and marked with dotted arrows. Positions −10, −40, and −70 are highlighted on top of the CCR209 sequence. Mutations are indicated in lowercase.

Tris, 45 mM boric acid, 1 mM EDTA), and electrophoresed for 1–1.5 h at 200 V/10 °C. Gels were vacuum dried and analyzed by autoradiography. Experimental conditions for DNase I footprinting matched those used for the gel shift assays. After incubation at 37 °C of the indicated DNA probe and protein(s), the mix was treated with 0.07 unit of DNase I for 2 min at 37 °C and then quenched with EDTA. DNA was ethanol-precipitated and run in 8 M urea and 8% or −6% polyacrylamide gels against G+A and C+T chemical sequencing ladders of the DNA probe used.

In Vitro Runoff Transcription—*In vitro* transcription reactions employed MxRNAP holoenzyme and CCR209 as template DNA. Transcription was carried out in a total reaction volume of 30 μl containing 0.5 nM CCR209, 25 mM Tris-HCl, pH 8.0, 5 mM $MgCl_2$, 100 mM KCl, 2 mM dithiothreitol, 200 ng/μl bovine serum albumin, 10% glycerol, 20 units of Protector RNase inhibitor (Roche), and 32 nM MxRNAP. When CarA was included (with or without CarS), it was incubated for 15 min at 30 °C with CCR209 prior to the addition of MxRNAP, followed by a further 15-min incubation at 30 °C. Transcription was then initiated by adding ATP, CTP, and GTP to 400 μM each, UTP to 20 μM, [α-^{32}P]UTP to 0.42 μM, in the presence of 50 μg/ml rifampicin to prevent reinitiation of transcription (33). Transcription was allowed to proceed at 30 °C for 15 min and then quenched with EDTA (final concentration 25 mM). Unincorporated nucleotides were eliminated by two successive ammonium acetate/ethanol precipitations. The precipitated products were analyzed by 8 M urea and 6% polyacrylamide gels followed by autoradiography.

In Vivo Analysis of Mutations in the P_B Promoter Region—Plasmid pMAR191 contains the CCR130 DNA segment fused to a transcriptional *lacZ* probe. A 1.5-kb *M. xanthus* DNA fragment in pMAR191 serves as target for plasmid integration into the chromosome by homologous recombination (22). pMAR191 also harbors a kanamycin resistance marker for positive selection. Site-directed mutagenesis by the PCR overlap extension method (36) was employed to generate plasmids pMR2672 (with CCR130-DMUT3) and pMR2854 (with CCR130-pIImut1). The presence of the desired mutation was confirmed by DNA sequencing. pMAR191, or its variants pMR2672 and pMR2854, were introduced into *M. xanthus* by electroporation. Integration of the plasmid was selected for on casitone-Tris plates containing 40 μg/ml kanamycin. The effects of specific mutations in CCR130 were monitored qualitatively on casitone-Tris plates containing 40 μg/ml 5-bromo-4-chloro-3-indolyl-β-D-galactopyranoside and quantitated by measurements of β-galactosidase activity as described previously (37).

RESULTS

Binding of CarA to the 130-bp carB Promoter Operator Probe and Its Fragments with 3′-End Truncations—All of the *cis*-acting elements essential for the correct regulation and expression of the *carB* promoter *in vivo* were shown to be located within a 130-bp segment spanning positions −102 to +28 relative to the transcription start site (22). We also determined that purified CarA binds to this 130-bp DNA fragment (CCR130; see Table I) *in vitro* to form two complexes in a concentration-dependent manner. At low CarA concentrations, a single retarded band was observed in gel shift assays, which in DNase I footprinting correlated with the protein being bound to an interrupted palindrome, pI, situated between positions −64 and −47 (footprint from position −70 to −41). With increasing CarA concentration, a second gel-retarded band appeared and became the predominant one at the highest protein concentrations used, and the DNase I footprint extended further downstream to around position −19. This second band was not observed with a shorter 64-bp DNA probe (CCR64), which lacks 66 bp starting from the 3′-end of CCR130 (22). This indicated that besides pI, additional CarA operator elements must exist in the DNA stretch which includes the −35 region and at least part of the −10 region of the *carB* promoter. Sequence analysis of the 130-bp segment highlighted two direct repeats (Table I; 22). One of these (D1) partially overlaps with pI; the second (D2) lies between the −11 and the −21 positions, and so within the segment that should include the second CarA operator element (see Fig. 2*A* and Table I). A precedent for such an arrangement of operator elements had been reported for the *dra-nupC-pdp* operon in *B. subtilis* (38, 39).

To define whether D2 (positioned between the −10 and −35 promoter regions) constitutes the second operator element, CCR130 was systematically truncated from its 3′-end to yield the following probes (see Fig. 2*A* and Table I): (i) CCR98, a 98-bp DNA fragment that retains D2 plus an additional 6 bp downstream; (ii) CCR87, an 87-bp DNA fragment where D2 is partially truncated; and (iii) CCR81, an 81-bp DNA fragment that completely lacks D2. As with CCR130, two gel-retarded bands were observed for CarA binding to CCR98, with the lower mobility one predominating at higher CarA concentrations (Fig. 2*B*). Thus, the second operator element is still present in CCR98. Similar results were obtained with the CCR87 probe, indicating that at least half of D2 can be eliminated without any noticeable effect on CarA·DNA complex formation (Fig. 2*C*). By contrast, with complete removal of D2 as in probe CCR81, primarily one retarded band was observed (Fig. 2*D*). However, the smearing out of the single band obtained with CCR81 at the highest CarA concentration, and not observed previously when CCR64 was used, indicates a tendency to form the second complex even in the complete absence of D2. This suggests, but does not prove on its own, that D2 may not be the second operator element. The inefficient formation of the lower mobility complex with CCR81 could then result from only partial removal of an as yet unidentified operator element. Alternatively, the second binding site could still be fully present in CCR81 but located too close to the 3′-end of the probe for a stable CarA-DNA interaction to occur.

Mutational Analysis of the Downstream Direct Repeat—To

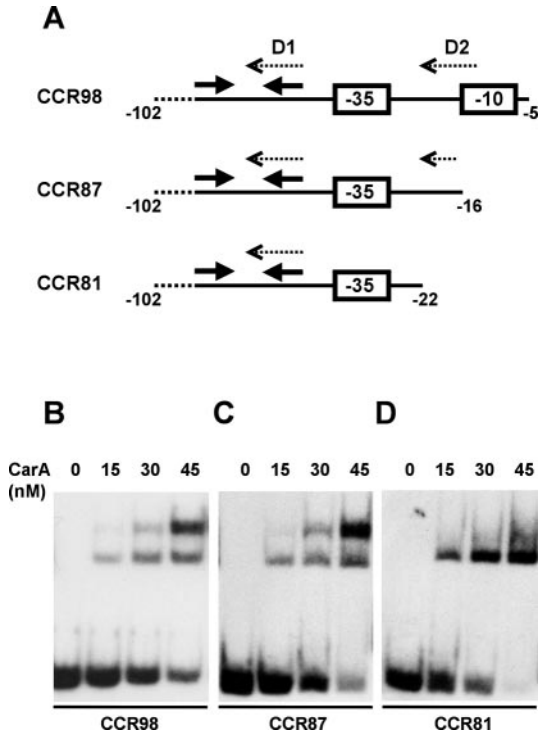

FIG. 2. **Binding of CarA to 3′-end truncated versions of CCR130 *in vitro*.** *A*, schematic representation of the 98-bp (CCR98), the 87-bp (CCR87), and the 81-bp (CCR81) probes corresponding to 3′-end truncations of CCR130. For sequences, see Table I. *Numbering* is relative to the transcription start site. The −10 and −35 promoter elements are indicated, the *solid arrows* refer to the inverted repeats, and the *dotted arrows* indicate the direct repeats D1 and D2 as labeled. *B*, *C*, and *D* are, respectively, EMSA of the binding to CCR98, CCR87, and CCR81 by CarA at the protein concentrations (in nM) indicated. Other experimental details are described under "Experimental Procedures." Note the two distinct retarded bands for CCR98 and CCR87 and the smearing with CCR81.

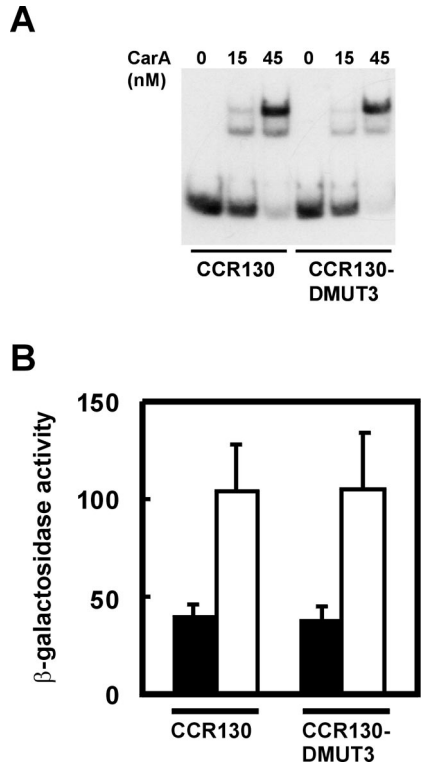

FIG. 3. **Effect of mutations in the downstream direct repeat of CCR130 on binding by CarA.** *A*, CarA binding to the CCR130 probe and its variant CCR130-DMUT3, which bears mutations in the downstream direct repeat D2, as probed by EMSA. Base changes in CCR130-DMUT3 are indicated in Table I. CarA concentrations (in nM) are shown, and the experimental conditions are detailed under "Experimental Procedures." *B*, measurements of β-galactosidase specific activities (in nmol/min/mg of protein) for *M. xanthus* strains bearing chromosomal integrations of plasmid pMR191, with a *lacZ* reporter gene under the control of the *carB* promoter CCR130 region (*left bars*) or pMR2672, with the *lacZ* gene under the control of the CCR130-DMUT3 variant (*right bars*) (Table I). Cell cultures were grown in the dark to exponential phase, divided in two, and one was grown in the dark and the other in the light for a further 8 h. The average of two independent determinations for samples taken after the 8-h incubation in the dark (*filled bars*) or in the light (*empty bars*) is shown.

investigate further the possibility that D2 is the second CarA operator element, we complemented the results obtained with the 3′-end truncated probes described in the previous section by resorting to site-directed mutagenesis. In designing the specific changes we considered D2 as consisting of two parts. One part would correspond to the first 4 bp that are identical in the two direct repeats. This part is immediately followed by a stretch of 6 bp that in the case of the upstream direct repeat D1 also constitutes the 3′-half of the palindrome pI, but differs at two positions in D2. Table I shows the specific mutations that were introduced in D2 to generate the CCR130-DMUT2 probe (which bears changes affecting the first 4 bp) and the CCR130-DMUT3 probe (which has been altered in the region that resembles the pI half-site). In the gel shift assay of Fig. 3*A*, the behavior of CCR130-DMUT3 at two different CarA concentrations matches that of the wild-type CCR130 probe, further reinforcing the idea that the second operator element does not map to this direct repeat.

To confirm that the apparently wild-type behavior of CCR130-DMUT3 *in vitro* correlates with normal operator activity *in vivo*, regulation of the *carB* promoter was assessed using a *lacZ* transcriptional probe fused to CCR130-DMUT3 (plasmid pMR2672, see "Experimental Procedures"). The *M. xanthus* wild-type strain DK1050 was electroporated with pMR2672, and electroporants having integrated the plasmid via homologous recombination were selected for on plates containing kanamycin. Several kanamycin-resistant electroporants were picked, and their β-galactosidase activity was compared with that of a control strain bearing the wild-type 130-bp fragment fused to the *lacZ* probe. Fig. 3*B* shows normal levels of repression and photoinduction at P_B for cells bearing the CCR130-DMUT3 mutant version, as judged by the levels of β-galactosidase activity observed for dark- and light-grown *M. xanthus* cultures relative to the control strain. Results similar to those shown *in vitro* and *in vivo* for CCR130-DMUT3 were obtained with CCR130-DMUT2 (data not shown). Thus, D2 is not part of the second CarA operator element, and its presence in the sequence may be purely fortuitous with no functional significance.

The Second CarA Operator Element Brackets the −35 Promoter Region—CCR87 was the smallest sized 3′-end-truncated variant of CCR130 tested, which yielded two gel-retarded bands (see above). Removal of an additional 6 bp at its 3′-end (CCR81) considerably diminished the formation of the lower mobility complex. However, the sequence of the six 3′-terminal bases in CCR87 can be changed without affecting the formation of the two CarA·DNA complexes (see previous section). Moreover, extension of CCR81 by 2 additional bp at the 3′-end was both necessary and sufficient to allow formation of the lower mobility species (data not shown). Together, these results suggest that the second CarA-binding site lies close to the 3′-end of CCR81, which may also explain why the second gel-retarded band could not be observed with this probe.

A 15-bp segment (positions −40 to −26) that brackets the

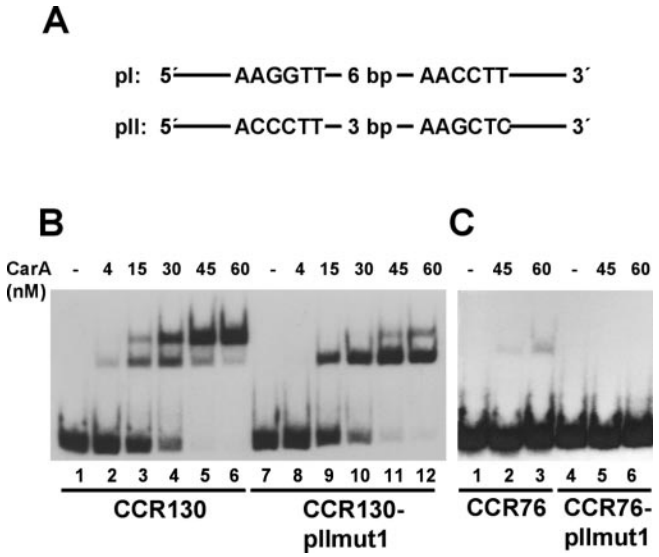

FIG. 4. **EMSA analysis of the second element of the CarA operator, pII.** *A*, sequences of the two halves and the separation between them for pI, the interrupted palindrome at −47 to −64, and pII, the interrupted pseudopalindrome (−26 to −40). For additional sequence information, see also Table I. *B*, EMSA analysis for CCR130 and the CCR130-pIImut1. *C*, EMSA analysis of the 76-bp probes lacking pI. CCR76 harbors the wild-type sequence, and CCR76-pIImut1 bears the mutation in pII equivalent to that in CCR130-pIImut1 (Table I). CarA concentrations (in nM) are indicated above each *lane*, *lane numbers* are at the *bottom*, and the DNA probe used is shown below the *solid line*.

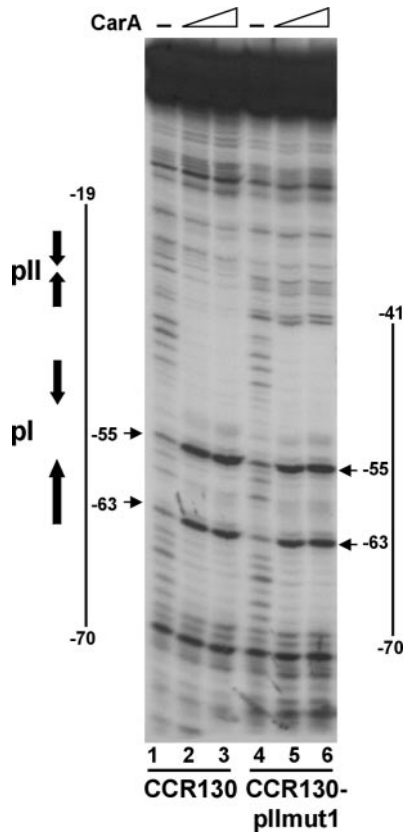

FIG. 5. **Analysis of the second element of the CarA operator by DNase I footprinting.** DNase I footprints for CarA binding to CCR130 and CCR130-pIImut1 under solution conditions equivalent to that in Fig. 4*B*. The segments of CCR130 and CCR130-pIImut1 protected by CarA against DNase I are shown by the *solid lines* to the *left* and *right* of the figure, respectively. pI and pII are shown by a *pair* of *arrows* facing one another, and the hypersensitive sites are indicated by *arrows*. The segments were assigned by G+A and C+T chemical sequencing ladders of the CCR130 (not shown; see also Ref. 22).

−35 promoter element shows some resemblance to pI. It can be viewed as an imperfect inverted repeat (pII) which, like pI, consists of two 6-bp half-sites but separated by 3 bp and not 6 as in pI (Fig. 4*A*). Relative to pI, three bp changes occur in the first half-site of pII and two in the second. To address whether pII contributes to CarA·DNA complex formation, both of its half-sites were mutated in the part that does not overlap with the −35 promoter hexamer (see Table I). The resulting 130-bp mutant probe, CCR130-pIImut1, was then compared with CCR130 in gel shift assays. As shown in Fig. 4*B*, elimination of pII provoked a marked decrease in the intensity of the lower mobility band, with a commensurate increase in that of the higher mobility complex (Fig. 4*B*, *lanes 7–12*) relative to the gel shift pattern obtained with the wild-type probe (Fig. 4*B*, *lanes 1–6*). A marginally detectable fraction of the low mobility complex persisted with the CCR130-pIImut1 probe at the highest CarA concentrations used (Fig. 4*B*, *lanes 11* and 12). Further evidence supporting the contribution of pII to CarA·DNA complex formation was obtained by gel shift analysis of a 76-bp truncated probe (CCR76) that lacks pI, and of the equivalent fragment with pII mutated (CCR76-pIImut1) (see Table I). Fig. 4*C* shows that with CCR76, only a single faint retarded band was observed at the highest CarA concentration used (60 nM; *lane 3*), which disappeared when the probe CCR76-pIImut1 was used (*lane 6*). This reinforces the inference that pII is a specific though low affinity binding site for CarA.

For a more detailed analysis of the effects derived from mutating pII, we also probed CarA·DNA complex formation *in vitro* by DNase I footprinting. With the wild-type CCR130 probe, the lower mobility complex in gel shift assays correlates with a DNase I footprint that extends from positions −70 to approximately −19 on the nontemplate strand, with hypersensitivities at −63 and −55 (Fig. 5, *lanes 1–3*, and Ref. 22). By contrast, under equivalent conditions, the DNase I footprint for CarA binding to CCR130-pIImut1 was reduced in its span: the footprint also started at position −70 but extended only up to −41 instead of −19 (Fig. 5, *lanes 4–6*). This pattern exactly matches that observed previously with the 3′-end truncated species CCR64, which lacks the 66-bp stretch that includes pII and D2 (22). We can then conclude that pII is the only other operator element that *in vitro* interacts with CarA. This element is essential in driving the formation of the lower mobility complex observed in gel shift assays, which we can now ascribe to occupancy of both pI and pII by CarA.

How pII is linked to operator activity *in vivo* was analyzed by monitoring expression of a *lacZ* reporter gene under the control of CCR130-pIImut1 (plasmid pMR2854; see "Experimental Procedures"). pMR2854 was introduced into the wild-type strain DK1050 by electroporation, and several electroporants were analyzed for β-galactosidase activity during growth in the dark and in the light. Fig. 6 shows the low expression levels from P_B in the dark and the 4-fold enhancement after an 8-h exposure to light for the wild-type probe CCR130. By contrast, *lacZ* expression in the dark was 10-fold higher for electroporants bearing the CCR130-pIImut1 mutant version relative to the wild-type (Fig. 6). Moreover, β-galactosidase activities estimated with the CCR130-pIImut1 *lacZ* probe in the dark and in the light (where it is about 1.3-fold higher; Fig. 6) are both comparable with the levels reported under equivalent conditions for a *car*A-deleted strain harboring the wild-type probe (22). In other words, mutating pII hampers CarA binding to be almost as ineffective as when CarA is absent or nonfunctional. Thus, we can then conclude that pII is critical for efficient *in vivo* repression of P_B in the dark and so is an essential operator element.

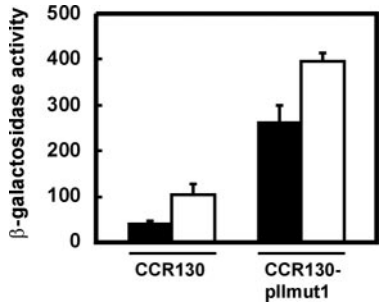

FIG. 6. **Constitutive expression of P_B in *M. xanthus* strains bearing pIImut1.** Measurements of β-galactosidase specific activities (in nmol/min/mg of protein) for *M. xanthus* strains bearing chromosomal integrations of: plasmid pMR191 with a *lacZ* reporter gene under the control of the *carB* promoter CCR130 region (*left bars*) or pMR2854 with the *lacZ* gene under the control of the CCR130-pIImut1 variant (*right bars*) (Table I) are shown. Cell cultures were grown in the dark to exponential phase and divided into two. One was grown for a further 8 h in the dark and the other in the light for the same period. *Numbers* are the average of two independent determinations for samples taken after the 8-h incubation in the dark (*filled bars*) or in the light (*empty bars*).

CarA-mediated Repression of carB and Its Antirepression by CarS—In vivo CarA down-regulates expression of P_B in the dark. Our *in vivo* and *in vitro* experiments show that CarA is a repressor that binds to a bipartite operator consisting of a high and a low affinity site (pI and pII, respectively). The mechanism of repression, however, still remained to be addressed. To gain insight into the molecular mechanism of P_B repression, we carried out DNA binding and runoff transcription assays *in vitro* using purified MxRNAP in the presence or absence of purified CarA. We also examined the consequences of the additional presence of purified CarS, the antirepressor of CarA.

The *carB* promoter shows a perfect match to the −35 consensus region for the *E. coli* σ^{70}-RNAP holoenzyme (TTGACA) but, as is often observed in the GC-rich *M. xanthus*, the −10 hexamer in P_B (TACCTC) diverges considerably from the consensus TATAAT in *E. coli*. We tested whether MxRNAP holoenzyme purified from vegetative cells binds to this region by gel shift and DNase I footprinting experiments and whether it was functionally competent to transcribe *in vitro*. MxRNAP was purified as described under "Experimental Procedures." The purified MxRNAP in SDS-PAGE showed the presence of the core α (43 kDa) and β/β′ subunits (at ~150 kDa), as well as a band at 105 kDa corresponding to the major vegetative σ^A, as verified in Western blots (see "Experimental Procedures").

The ability of MxRNAP to bind stably to CCR130 was first assayed by gel shift experiments after a 30-min incubation at 37 °C, to allow for open complex formation. Fig. 7*A* shows a single retarded band whose intensity increased as the concentration of MxRNAP was raised. This complex was resistant to competition by polyanion heparin added after the 30-min incubation (Fig. 7*A*, *lane 6*) but failed to form when heparin was mixed with CCR130 prior to the addition of MxRNAP (Fig. 7*A*, *lane 7*). Heparin has been shown to dissociate nonspecific and closed promoter-RNAP complexes (40). Thus, the observed competitor-resistant complex would likely correspond to an open MxRNAP·P_B complex. This was supported further by the pattern obtained in DNase I protection assays. Studies with *E. coli* RNAP have reported DNA structural changes linked to open complex formation that can be probed by footprinting and are manifested by an expansion of the footprint toward the transcribed region. A span of the total footprint from about −57/−52 to +20/+25 is thus indicative of open complex formation (41–44). Similar DNase I protection patterns have been reported to reflect open complex formation with *B. subtilis* RNAP (45–47). The MxRNAP·DNA complex formed at 37 °C was therefore probed by DNase I footprinting. The 3′-end of CCR130 (position +28) is close to the reported downstream boundary for the region protected by *E. coli* or *B. subtilis* RNAP open complexes. So, to visualize better the limits of the footprint produced by MxRNAP, a 209-bp DNA fragment spanning positions −102 to +107 (CCR209; Table I) was used in the experiments shown in Fig. 7*B*. With increasing concentrations of MxRNAP, a footprint of about 79 bp spanning P_B became evident on the nontemplate (Fig. 7*B*, *lanes 1–4*) as well as on the template strand (Fig. 7*B*, *lanes 6–9*). On the nontemplate strand, a footprint from about −58 to +20 with slight enhancement of DNase I cleavage at −26 and −45 was observed. On the template strand, the footprint extended from about −60 to +19, with hypersensitivities at positions −49 and −25. The observed DNase I footprint resembles in its span those obtained for *E. coli* or *B. subtilis* open RNAP·promoter complexes (to our knowledge, this is the first footprint reported for MxRNAP-promoter binding). These results further reinforce the idea that MxRNAP is capable of recognizing P_B and of undergoing the necessary conformational changes to form a stable open complex at this promoter.

The ability of MxRNAP to transcribe from P_B was analyzed by single round runoff transcription assays. First, the CCR209 DNA fragment was incubated with MxRNAP to allow for open complex formation. Transcription was then initiated by the addition of ATP, CTP, GTP, and UTP/[^{32}P]UTP mix with rifampicin included to prevent reinitiation of transcription. After 15 min, the reaction was quenched, and the products were analyzed by gel electrophoresis followed by autoradiography. Based on the transcription start site identified previously by primer extension (16), a 107-nucleotide runoff product would be expected. A transcript of the correct size was observed (Fig. 7*C*, *lane 1*). These results corroborate that the purified MxRNAP is competent to initiate transcription at the expected start site. We then proceeded to study the effect of CarA on P_B transcription and how this was affected by the additional presence of CarS. As shown in Fig. 7*C* (*lanes 2–4*), transcription from P_B was gradually shut off as the concentration of CarA was raised. These experiments, where the addition of CarA preceded that of MxRNAP, demonstrate the repressor activity of CarA. The inhibitory effect of CarA on transcription by MxRNAP was relieved when CarS was also present in the reaction, consistent with it being the antirepressor of CarA (Fig. 7*C*, compare *lanes 6* and *7*).

The molecular basis for CarA-mediated repression of P_B was investigated by gel shift and DNase I footprinting assays. Fig. 8*A* shows the effect of CarA on MxRNAP open complex formation, as analyzed by gel retardation. When CCR130 was incubated with increasing concentrations of CarA prior to the addition of MxRNAP, the yield of the MxRNAP·CCR130 band decreased progressively in a manner concomitant with the appearance of the lower mobility CarA·CCR130 complex (Fig. 8*A*, compare *lane 2* with *lanes 3–8*). At the maximum CarA concentration used, all of the CCR130 probe was bound to CarA with very little, if any, detected as MxRNAP complex (Fig. 8*A*, *lane 8*). Equivalent results were obtained when CCR130 was incubated with MxRNAP first or when added simultaneously with the maximum amount of CarA used (Fig. 8*A*, *lanes 10* and *11*). As seen in *lane 9* of Fig. 8*A*, the addition of sufficient CarS to abolish CarA·CCR130 binding restored complex formation by MxRNAP. These observations at 37 °C were unaltered when the binding reactions were performed at 4 °C (data not shown). At this lower temperature, the MxRNAP·CCR130 closed complex would be expected to be the predominant form, as was confirmed by sensitivity to heparin competition. Together, these results suggest that CarA inhibits the formation of the

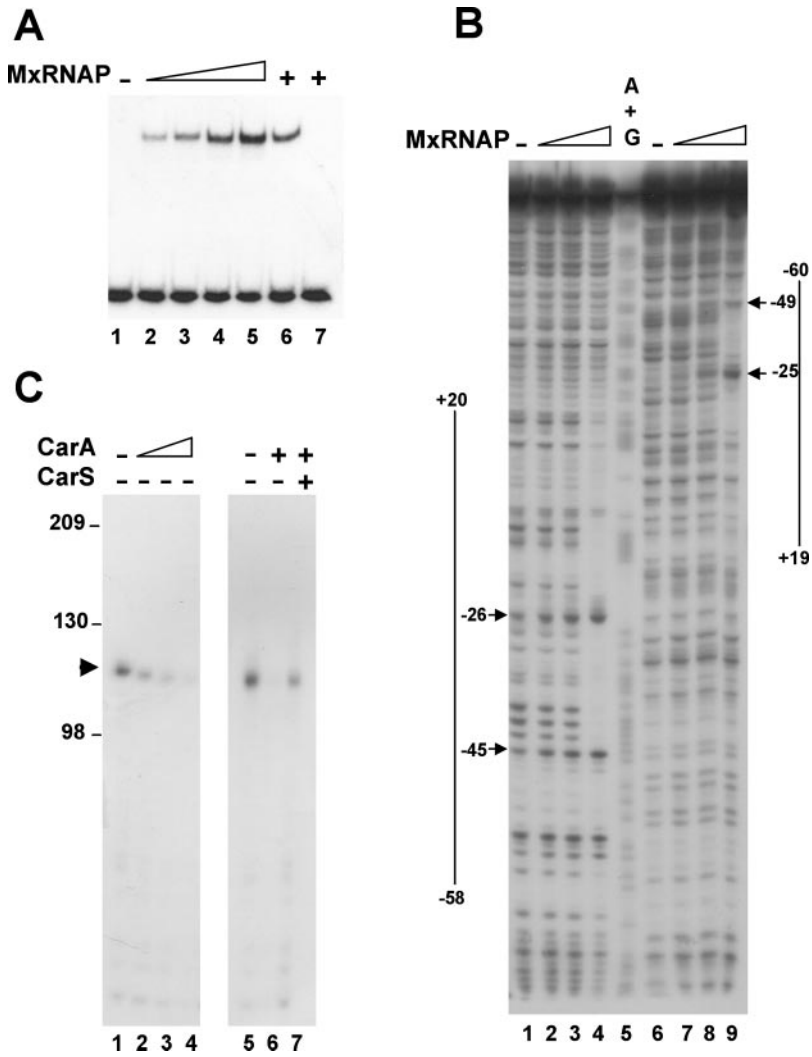

FIG. 7. ***In vitro* analysis of MxRNAP interactions at the *carB* promoter region.** *A*, *lanes 2–5*, increasing concentrations of MxRNAP (16, 32, 64, and 130 nM) and CCR130 were incubated at 37 °C for 30 min to allow for open complex formation and then analyzed by EMSA. *Lane 6*, 1 μg of competitor heparin was added after incubation of 130 nM MxRNAP with CCR130 at 37 °C for 30 min. *Lane 7*, same as in *lane 6* except that heparin was mixed with CCR130 before the addition of MxRNAP. *B*, DNase I footprinting analysis of MxRNAP binding to CCR209. *Lanes 2–4* show the DNase I protection pattern on the nontemplate strand for increasing concentrations of MxRNAP (16, 32, and 64 nM) and *lanes 7–9* for that on the template strand. *Lane 6*, A+G chemical sequencing ladder of the template strand. The span of the footprint is indicated with a *solid line* for the nontemplate strand (on the *left*) and for the template strand (on the *right*). DNase I-hypersensitive sites are marked with *arrows*. *C*, *in vitro* transcription runoff analysis using CCR209. *Lanes 1* and *5*, 32 nM MxRNAP. *Lanes 2–4*, 32 nM MxRNAP and increasing concentrations of CarA (15, 30, and 60 nM). *Lane 6*, 32 nM MxRNAP and 60 nM CarA. *Lane 7*, 32 nM MxRNAP, 60 nM CarA, and excess (900 nM) CarS. The *numbers* on the *left side* of *C* indicate size markers; the runoff transcript is shown by the *arrowhead*.

closed complex by efficiently competing with MxRNAP to occlude its binding to P_B.

If CarA does block transcription by steric hindrance, the MxRNAP DNase I footprint should be replaced by that characteristic for CarA, when the latter is also present at a sufficiently high concentration. In reactions with MxRNAP and CarA, the footprint described above for MxRNAP open complex at P_B progressively disappeared with increasing CarA concentrations (Fig. 8*B*, compare *lane 2* with *lanes 4–8*). At a concentration of CarA where both pI and pII would normally be occupied, the MxRNAP footprint was replaced by that corresponding to CarA alone (Fig. 8*B*, *lane 8*). On addition of CarS, the MxRNAP footprint became evident again (Fig. 8*B*, *lane 9*). These results indicate that CarA down-regulates transcription from P_B by interfering with MxRNAP-promoter binding and that this effect is counteracted by CarS.

DISCUSSION

The Bipartite CarA Operator—Expression of the structural genes in the *carB* operon is repressed by CarA in the dark. To elucidate the molecular details of how CarA acts, we undertook a complete description of its cognate operator. Our dissection of the specific binding site for the CarA repressor has revealed it to be a bipartite operator. One module, pI, is an 18-bp segment upstream of the promoter that displays dyad symmetry, with 6-bp repeats flanking a 6-bp intervening stretch. The design of this module resembles in some respects that reported previously for the operator of MerR, the prototypical member of a family of transcriptional regulators whose DNA binding domain shows sequence similarity to the N-terminal domain of CarA (16). In the absence of Hg(II), MerR represses expression of the mercury resistance operon *merTP(C)AD* but activates its expression when Hg(II) is present. Both MerR and Hg-MerR contact a symmetrical operator region that is an 18-bp interrupted perfect palindrome like pI but consisting of a 7-bp inverted repeat separated by 4 bp (for review, see Ref. 48). Unlike pI, which is located upstream of P_B, the *mer* operator falls within the −37 and −10 promoter regions. Moreover, the single module arrangement of the *mer* operator contrasts with a bipartite organization of the CarA operator, where a second operator element that would lie within the promoter region was inferred from CarA-DNA binding in *in vitro* studies (22). Based on sequence analysis and by analogy with the operator design for the *B. subtilis dra-nupC-pdp* operon, we had initially proposed a direct repeat (D2) located in the spacer region between the −35 and −10 hexamers as the possible second CarA binding site (22). We demonstrate here using *in vitro* DNA binding assays as well as *in vivo* expression analysis that D2 does not contribute to CarA operator activity, and its occurrence appears to be purely happenstance. Instead, the second module that constitutes the operator (pII) is positioned 6 bp downstream of pI and consists of a 15-bp interrupted imperfect palindrome whose central core is the −35 promoter hexamer TTGACA. Separated by 3 bp (rather than 6 as in pI) are the two outlying 6-bp stretches of pII that resemble somewhat the

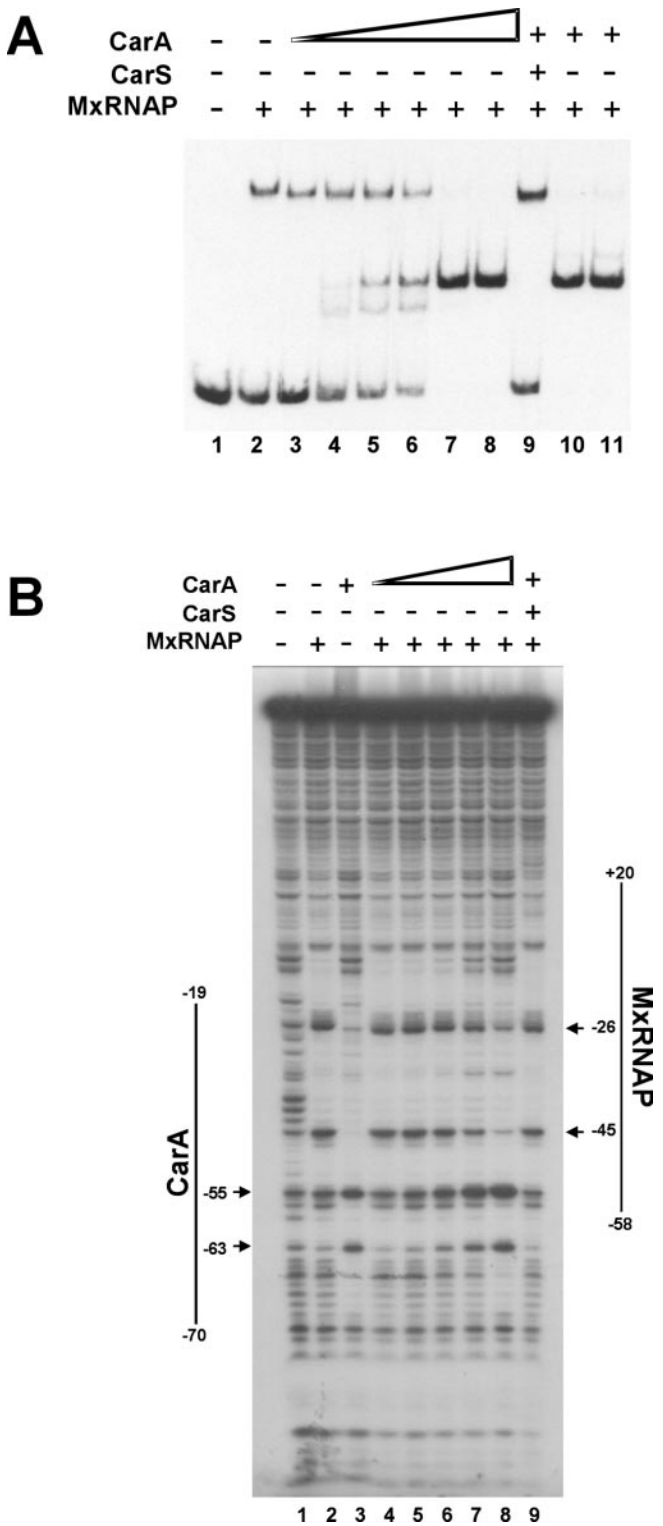

FIG. 8. **Analysis of repression and antirepression of P_B by CarA and CarS *in vitro*.** *A*, EMSA analysis of MxRNAP·CCR130 open complex formation by incubation at 37 °C for 30 min with CarA added in increasing concentrations (0, 3, 7, 15, 40, 45, and 60 nM) to the reaction mix before the addition of 64 nM MxRNAP (*lanes 2–8*). *Lane 9* is identical to *lane 8* except that 900 nM CarS was added together with 60 nM CarA before introducing MxRNAP. *Lane 10* corresponds to CCR130 incubated with 64 nM MxRNAP before the addition of 60 nM CarA, and *lane 11* to 60 nM CarA and 64 nM MxRNAP added simultaneously. *B*, *lanes 4–8*, DNase I footprinting analysis of 64 nM MxRNAP binding to CCR209 with increasing CarA concentrations (7, 15, 30, 45, and 60 nM). *Lane 2*, 64 nM MxRNAP alone. *Lane 3*, 60 nM CarA alone. *Lane 9*, 64 nM MxRNAP, 60 nM CarA, and 900 nM CarS. The features of the footprint generated by CarA are displayed on the *left*, and those of MxRNAP are on the *right*.

corresponding ones in pI. When CarA is bound to pI alone, a DNase I footprint precisely centered around this operator site and with a total span of 30 bp is observed (Fig. 4*D*; 22). Occupation of pII by CarA (when pI is bound as well) is also characterized by a DNase I protection pattern that extends beyond the downstream half-site by about 6 bp. In addition, stable cooperative binding of CarA to pII is abolished when DNA probes with less than 6-bp from the downstream half-site are used. Altogether, these results suggest that nonspecific contacts with 6-bp on each side of the recognition sites may be necessary to facilitate stable CarA binding.

The intrinsic affinity of CarA for pI is markedly higher than for pII as deduced from *in vitro* binding assays using probes containing the sites in isolation. Moreover, when the two sites are present as in the intact CarA operator, CarA binds first to pI and only then, in a cooperative manner, to pII. Mutations that cause deviations from the perfect dyad symmetry in pI dramatically decrease CarA binding (22). Thus, one likely factor accounting for the lower affinity of CarA for pII is the absence of perfectly inverted repeats at this site. Another factor that could also contribute to the decreased affinity of pII for CarA is its smaller 3-bp spacer, which would alter the register between the two half-sites, as well as diminish the size of the binding site. Despite its lower affinity, pII appears to be the checkpoint for efficient *carB* repression *in vivo*, the binding of CarA to pI being nevertheless a prerequisite for effective binding to pII. The cooperative binding of regulatory proteins to nucleic acids is an essential feature of many regulatory networks identified to date. In some cases, cooperativity results from enhancement of the local concentration of the binding protein in the vicinity of multiple binding sites (for review, see Ref. 49). Alternatively, a protein tightly bound to a strong site can facilitate binding to a weaker site through the formation of a protein-protein complex that already exists in the absence of DNA (50) or assembles specifically and solely on DNA (51). CarA can interact with itself, and this appears to be mediated by its 209-residue C-terminal region (22). The property of CarA to oligomerize could be relevant in binding to the strong pI site, probably as a dimer given the dyadic symmetry of this site. This would be reminiscent of various phage and bacterial transcriptional repressors that bind as homodimers using a helix-turn-helix motif from each monomer to interact with one half-site of symmetry-related DNA (52). Oligomerization could also play an important role in driving the binding of CarA to the low affinity site pII. Indeed, deletion of its oligomerization domain leads to a constitutive light-independent expression of P_B *in vivo* (55). The particular spatial arrangement and the differential repressor binding affinities of pI and pII in the design of the CarA operator may have evolved to achieve the proper fine-tuning in the control of *carB* expression, as discussed next.

Mechanism for CarA-mediated Down-regulation of P_B—The *carB* promoter sequence reveals it to be of the σ^{70}-type, with a consensus *E. coli* TTGACA −35 hexamer but whose −10 hexamer varies from the consensus, as is frequently the case with *M. xanthus*. We have shown that purified MxRNAP holoenzyme containing the major vegetative σ^A factor binds to this promoter to form a stable, heparin-resistant, open MxRNAP-promoter complex *in vitro*. The DNase I footprint obtained with this MxRNAP·P_B complex extends from about −58 to +20 on the nontemplate strand and from about −60 to +19 on the template strand. A similar span has been observed with *E. coli* or *B. subtilis* RNAP holoenzymes harboring their respective major vegetative σ factor when bound to cognate promoters. Moreover, the MxRNAP·P_B complex is transcriptionally competent as confirmed in runoff transcription assays that yielded a transcript of the expected size. CarA abolished runoff tran-

scription, and this was counteracted by CarS, thereby reproducing *in vitro* the action of CarA and CarS inferred from *in vivo* experiments.

Gel retardation analysis of the specific association between P_B and MxRNAP revealed that CarA, when bound to both of its operator subsites, very effectively thwarts MxRNAP·P_B complex formation. This efficient impediment to MxRNAP generated by CarA occurs irrespective of the order of addition of the two proteins or whether the two are introduced to the reaction mix at the same time. Moreover, the outcome of these *in vitro* assays was indistinguishable when the binding reaction was carried out at 37 °C, where the more stable heparin-resistant open complexes predominate, or at 4 °C, where the principal species is the less stable, closed, heparin-sensitive complex. A far greater affinity of CarA for its operator relative to that of MxRNAP for P_B in the closed as well as in the open complex could account for these observations: (i) CarA, when added simultaneously with MxRNAP, would compete for free operator DNA far more effectively than MxRNAP for P_B; (ii) when added to preformed MxRNAP·P_B complexes, effective competition by the higher affinity CarA-operator binding could act by trapping free DNA resulting from the dissociation of the open or closed MxRNAP·P_B complex. DNase I footprinting analysis under equivalent conditions showed that the operator-bound CarA does not coexist with the MxRNAP·P_B complex. This mutually exclusive binding of CarA and MxRNAP to their specific sites is consistent with CarA sterically hindering access of MxRNAP to P_B. Thus, CarA would belong to the class of transcriptional repressors that includes, among others, the classical paradigms LacI, λcI, and LexA repressors (4, 53, 54), whose operators at least partially overlap the promoter and occlude RNAP on repressor-operator binding.

All our current data therefore lead us to the following model for light-regulated expression of P_B. In the dark, CarA is present in amounts sufficient to occupy in a cooperative manner both of its operator subsites and thereby impede MxRNAP binding. Overexpression of CarS upon illumination would counteract this inhibitory effect through competition with CarA·DNA binding via direct protein-protein interactions with CarA. *In vitro*, CarS dismantles CarA-operator complexes by first evicting CarA from its low affinity subsite (which we have shown in this study to be pII), and only then from the higher affinity pI (22). The constitutive phenotype observed for mutants in the lower affinity operator element pII leads us to infer that, *in vivo*, the release of CarA from this subsite would be sufficient to allow access of MxRNAP and so bring about derepression. Thus, the CarA operator design may have evolved to match the needs for both a rapid as well as an effective response to light. The complete occupancy of the operator that is essential for efficient repression in the dark would be enhanced by the cooperative nature of CarA binding to pI leading on to pII. On the other hand, derepression of *carB* on exposure to light would be achieved most rapidly when the transcriptional blockage imposed by CarA bound to pII is easily dismembered, because of its low affinity, by CarS.

Acknowledgments—We thank J. A. Madrid for technical assistance. We also acknowledge the instrumental facilities at Centro de Investigaciones Biológicas (Madrid) for DNA sequencing.

REFERENCES

1. Rojo, F. (1999) *J. Bacteriol.* **181,** 2987–2991
2. Lloyd, G., Landini, P., and Busby, S. (2001) *Essays Biochem.* **37,** 17–31
3. Ptashne, M. (1986) *A Genetic Switch*: *Gene Control and Phage λ*, Blackwell Scientific Publications, Cambridge, MA
4. Schlax, P. J., Capp, M. W., and Record, M. T., Jr. (1995) *J. Mol. Biol.* **245,** 331–350
5. Lee, Y. S., and Hwang, D. S. (1997) *J. Biol. Chem.* **272,** 83–88
6. Rojo, F., and Salas, M. (1991) *EMBO J.* **10,** 3429–3438
7. Choy, H., and Adhya, S. (1996) in *Escherichia coli and Salmonella (*Neidhardt, F., ed) Vol. 1, pp. 1287–1299, American Society for Microbiology Press, Washington, D. C.
8. O′Halloran, T. V., Frantz, B., Shin, M. K., Ralston, D. M., and Wright, J. G. (1989) *Cell* **56,** 119–129
9. Williams, D. R., Motallebi-Veshareh, M., and Thomas, C. M. (1993) *Nucleic Acids Res.* **21,** 1141–1148
10. Smith, T. L., and Sauer, R. T. (1996) *Proc. Natl. Acad. Sci. U. S. A.* **93,** 8868–8872
11. Choy, H., and Adhya, S. (1992) *Proc. Natl. Acad. Sci. U. S. A.* **89,** 11264–11268
12. Monsalve, M., Mencía, M., Rojo, F., and Salas, M. (1996) *EMBO J.* **15,** 383–391
13. Hodgson, D. A., and Murillo, F. J. (1993) in *Myxobacteria II* (Dworkin, M., and Kaiser, D., eds) pp. 157–181, American Society for Microbiology Press, Washington, D. C.
14. Ruiz-Vázquez, R. M., Fontes, M., and Murillo, F. J. (1993) *Mol. Microbiol.* **10,** 25–34
15. Fontes, M., Ruiz-Vázquez, R. M., and Murillo, F. J. (1993) *EMBO J.* **12,** 1265–1275
16. Botella, J. A., Murillo, F. J., and Ruiz-Vázquez, R. M. (1995) *Eur. J. Biochem.* **223,** 238–248
17. Fontes, M., Galbis-Martínez, L., and Murillo, F. J. (2003) *Mol. Microbiol.* **47,** 561–571
18. Gorham, H. C., McGowan, S. J., Robson, P. R. H., and Hodgson, D. A. (1996) *Mol. Microbiol.* **19,** 171–186
19. Martínez-Argudo, I., Ruiz-Vázquez, R. M., and Murillo, F. J. (1998) *Mol. Microbiol.* **30,** 883–893
20. Browning, D. F., Whitworth, D. E., and Hodgson, D. A. (2003) *Mol. Microbiol.* **48,** 237–251
21. Whitworth, D. E., and Hodgson, D. A. (2001) *Mol. Microbiol.* **42,** 809–819
22. López-Rubio, J. J., Elías-Arnanz, M., Padmanabhan, S., and Murillo, F. J. (2002) *J. Biol. Chem.* **277,** 7262–7270
23. Nicolás, F. J., Ruiz-Vázquez, R. M., and Murillo, F. J. (1994) *Genes Dev.* **8,** 2375–2387
24. Nicolás, F. J., Cayuela, M. L., Martínez-Argudo, I., Ruiz-Vázquez, R. M., and Murillo, F. J. (1996) *Proc. Natl. Acad. Sci. U. S. A.* **93,** 6881–6885
25. Padmanabhan, S., Elías-Arnanz, M., Carpio, E., Aparicio, P., and Murillo, F. J. (2001) *J. Biol. Chem.* **276,** 41566–41575
26. Cayuela, M. L., Elías-Arnanz, M., Peñalver-Mellado, M., Padmanabhan, S., and Murillo, F. J. (2003) *J. Bacteriol.* **185,** 3527–3537
27. Moreno, A. J., Fontes, M., and Murillo, F. J. (2001) *J. Bacteriol.* **183,** 557–569
28. Martínez-Laborda, A., and Murillo, F. J. (1989) *Genetics* **122,** 801–806
29. McGowan, S. J., Gorham, H. C., and Hodgson, D. A. (1993) *Mol. Microbiol.* **10,** 713–735
30. Ruiz-Vázquez, R. M., and Murillo, F. J. (1984) *J. Bacteriol.* **160,** 818–821
31. Bretscher, A. P., and Kaiser, D. (1978) *J. Bacteriol.* **133,** 763–768
32. Sambrook, J., and Russell, D. W. (2000) *Molecular Cloning: A Laboratory Manual*, 3rd Ed., Cold Spring Harbor Laboratory Press, Cold Spring Harbor, NY
33. Rudd, K. E., and Zusman, D. R. (1982) *J. Bacteriol.* **151,** 89–105
34. Inouye, S. (1990) *J. Bacteriol.* **172,** 80–85
35. Biran, D., and Kroos, L. (1997) *Mol. Microbiol.* **25,** 463–472
36. Ho, S. N., Hunt, H. D., Horton, R. M., Pullen, J. K., and Pease, L. R. (1989) *Gene* (*Amst.*) **77,** 51–59
37. Balsalobre, J. M., Ruiz-Vázquez, R. M., and Murillo, F. J. (1987) *Proc. Natl. Acad. Sci. U. S. A.* **84,** 2359–2362
38. Zeng, X., and Saxild, H. H. (1999) *J. Bacteriol.* **181,** 1719–1727
39. Zeng, X., Saxild, H. H., and Switzer, R. L. (2000) *J. Bacteriol.* **182,** 1916–1922
40. Straney, S. B., and Crothers, D. M. (1987) *Biochemistry* **26,** 5063–5070
41. Spassky, A., Kirkegaard, K., and Buc, H. (1985) *Biochemistry* **24,** 2723–2731
42. Schickor, P., Metzger, W., Wladyslaw, W., Lederer, H., and Heumann, H. (1990) *EMBO J.* **9,** 2215–2220
43. Mecsas, J., Cowing, D. W., and Gross, C. A. (1991) *J. Mol. Biol.* **220,** 585–597
44. Craig, M. L., Suh, W. C., and Record, M. T., Jr. (1995) *Biochemistry* **14,** 15624–15632
45. Whipple, F. W., and Sonenshein, A. L. (1992) *J. Mol. Biol.* **223,** 399–414
46. Elías-Arnanz, M., and Salas, M. (1999) *Genes Dev.* **13,** 2502–2513
47. Camacho, A., and Salas, M. (2001) *J. Biol. Chem.* **276,** 28927–28932
48. Summers, A. O. (1992) *J. Bacteriol.* **174,** 3097–3101
49. Müller-Hill, B. (1998) *Mol. Microbiol.* **29,** 13–18
50. Courey, A. J. (2001) *Curr. Biol.* **11,** R250–R252
51. Ciubotaru, M., and Koudelka, G. B. (2003) *Biochemistry* **42,** 4253–4264
52. Huffman, J. L., and Brennan, R. G. (2002) *Curr. Opin. Struct. Biol.* **12,** 98–106
53. Hawley, D. K., Johnson, A. D., and McClure, W. R. (1985) *J. Biol. Chem.* **260,** 8618–8626
54. Bertrand-Burggraf, E., Hurstel, S., Daune, M., and Schnarr, M. (1987) *J. Mol. Biol.* **193,** 293–302
55. Pérez-Marín, M. C., López-Rubio, J. J., Murillo, F. J., Elías-Arnanz, M., and Padmanabhan, S. (May 25, 2004) *J. Biol. Chem.* 10.1074/jbc.M405225200

Operator Design and Mechanism for CarA Repressor-mediated Down-regulation of the Photoinducible *carB* Operon in *Myxococcus xanthus*

José Juan López-Rubio, S. Padmanabhan, Jose María Lázaro, Margarita Salas, Francisco José Murillo and Montserrat Elías-Arnanz

J. Biol. Chem. 2004, 279:28945-28953.
doi: 10.1074/jbc.M403459200 originally published online April 28, 2004
